Optimization of the Substitution Pattern of 1,3-Disubstituted Imidazo[1,5-a]Pyridines and -Quinolines for Electro-Optical Applications

Georg Albrecht, Carina Rössiger, Jasmin Martha Herr, Harald Locke, Hisao Yanagi, Richard Göttlich, and Derck Schlettwein*

A series of recently synthesized 1,3-disubstituted imidazo[1,5-a]pyridines (IPs) and -quinolines (IQs) targeting at increased efficiency of luminescence is investigated. The properties of molecules in solution as well as their change in the solid state are reported and assessed regarding possible application in organic electronics. The influence of increased ring size by substitution, e.g., exchanging phenyl to naphthalenyl, as well as pyridyl to quinolinyl moieties, and by means of a larger IQ fluorophore is discussed. A higher oscillator strength and quantum yield can be achieved. Frontier orbital energies are estimated based on cyclic voltammetry and density functional theory (DFT) calculations. Single crystals of molecules are grown. A red-shift in the photoluminescence spectra found for crystals of IQs compared with those in solution is proposed to be caused by intermolecular coupling based on the parallel stacking of the enlarged fluorophore units. Thin films deposited by physical vapor deposition exhibit similar effects, showing promise as active layers in organic light-emitting diodes (OLEDs). An amorphous morphology is inferred for these films from both spectral broadening in photoluminescence and atomic force microscopy. An OLED test structure is prepared, using the most efficient IQ lumophore and demonstrating the feasibility of obtaining electroluminescence from such thin films.

1. Introduction

Organic fluorophores are well-established functional molecules, used as luminescent probes in medicine and biology,[1,2] as photonic materials,[3] or in organic electronics.[4] Since the first work on organic light-emitting diodes (OLEDs) by Tang and VanSlyke,[5] such devices have attracted significant attention and are now part of state-of-the-art displays.[6–11] In this context,

key performance parameters as well as new unique characteristics can be influenced or introduced by novel fluorophores.

Blue light-emitting 1,3-disubstituted imidazo[1,5-a]pyridines (IPs) and their imidazo[1,5-a]quinoline (IQ) homologues show quantum yields up to 44%, possess large Stokes shifts, and can be prepared by facile synthetic methods.[12–17] Also, IQs have exhibited suitable material properties for application in OLEDs.[14,15] Using 1-(pyridin-2-yl)-3-(quinolin-2-yl)imidazo[1,5-a]quinoline in a layer architecture with typical contact materials, blue OLEDs were prepared recently.[18] The substitution with different functional groups up to now has mainly been studied on the IP core.[12–14,17,19–22] The increase in the size of the π-system at the chromophore unit can affect quantum yield[23] and absorbance wavelength, determined by the gap between frontier orbitals.[24,25] In addition, such a change in orbital energy might be influenced by the twisting of the π-system,[26] as a consequence of introduced functional moieties perturbing conformation. In the context of improving optical properties, the further exploration of such effects on IP derivatives and an extension of such a study on the group of IQs are, therefore, useful in an assessment for application in OLEDs.

Consequently, in addition to molecular properties, studies on fluorophores in the solid state are required. Single crystals consist of highly ordered organic molecules, providing insight

Dr. G. Albrecht, Prof. D. Schlettwein
Institute of Applied Physics
Justus Liebig University (JLU) Giessen
Heinrich-Buff-Ring 16, 35392 Giessen, Germany
E-mail: schlettwein@uni-giessen.de

The ORCID identification number(s) for the author(s) of this article can be found under https://doi.org/10.1002/pssb.201900677.

C. Rössiger, J. M. Herr, H. Locke, Prof. R. Göttlich
Institute for Organic Chemistry
Justus Liebig University (JLU) Giessen
Heinrich-Buff-Ring 17, 35392 Giessen, Germany

Prof. H. Yanagi
Graduate School of Science and Technology
Nara Institute of Science and Technology (NAIST)
8916-5 Takayama, Ikoma, Nara 630-0192, Japan

to molecular interaction at close proximity. The π-systems of molecules may interact, leading to π–π stacking.[27] Therefore, charge carrier mobility is affected by the crystalline structure[27,28] and in particular, the coupling of electronic wave functions, which is depending on molecular arrangement that influences luminescence energy and intensity compared with isolated or dissolved molecules.[29–31] In contrast to crystals, but depending on the preparation conditions, thin films (TFs) of organic molecules are often amorphous rather than crystalline. Charge carrier mobility in such amorphous layers, which is based on hopping transport, is also dependent on the extent of electronic coupling.[32] Furthermore, to effectively inject charge carriers into TFs, knowledge on the energy of the frontier orbitals is needed. The work function of adjacent layers has to be close in energy to the respective orbital to minimize the barrier for the injection of charge carriers. Physical vapor deposition (PVD) serves as a suitable method to prepare such TFs and interfaces because it often leads to pure and homogeneous layers.[33,34] Despite advantages of alternative solvent-based film preparation, PVD is, therefore, often also used in technical device preparation.[34]

In this work, the step-wise change of physical properties was investigated for a range of five differently substituted IPs and IQs each. Absorption and emission spectra as well as quantum yields were measured in solution and interpreted based on density functional theory (DFT) calculations. The effects on the energy of the highest-occupied molecular orbital (HOMO) were studied by cyclic voltammetry and analyzed. For a representative choice of molecules, single crystals were grown and TFs were prepared by PVD. Time-resolved and steady-state photoluminescence of the molecules was used to assess the degree of intermolecular coupling. Furthermore, thin-film morphology was derived from the spectroscopic measurements and verified by atomic force microscopy (AFM). To demonstrate applicability to OLED technology, a simple test device with the most efficient lumophore in the active layer was built.

2. Results and Discussion

The investigated molecules **IP1–IP5** and **IQ1–IQ5** are shown in **Table 1** with their structure formula in **Figure 1**. Different moieties were chosen at R and R′ to study their effects on molecular

Table 1. Molecules investigated in this study. R and R′ are shown in Figure 1.

	R	R′
IP1	Phenyl	Phenyl
IP2	Phenyl	4-Methoxyphenyl
IP3	Pyridin-2-yl	Pyridin-2-yl
IP4	Naphthalenyl	Phenyl
IP5	Naphthalenyl	Pyridin-2-yl
IQ1	Naphthalenyl	Phenyl
IQ2	Phenyl	Pyridin-2-yl
IQ3	Quinolin-2-yl	Pyridin-2-yl
IQ4	Naphthalenyl	4-Fluorophenyl
IQ5	Quinolin-2-yl	4-Fluorophenyl
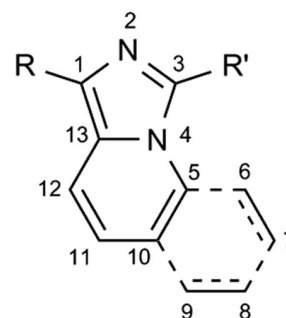
Figure 1. Structure formula of the investigated 1,3-disubstituted **IP** (black) and **IQ** (added gray area). R and R′ are shown in Table 1.

properties. In particular, the distribution of the conjugated π-orbitals is of interest. This property changes when comparing **IP1** with **IP4**, for example, going from a phenyl to a naphthalenyl moiety at R, or from **IP4** to **IQ1**, exchanging the IP to an IQ core. The phenyl and naphthalenyl moieties furthermore are replaced by pyridyl and quinolinyl groups, e.g., when comparing **IP1** with **IP3** or **IQ1** with **IQ2**, which can, for example, influence orbital energies.[35] Fluorination (**IQ4** and **IQ5**) as well as methoxylation (**IP2**) have shown to improve optical properties in a previous work.[21] As some characteristics of solutions and crystals of **IQ3** have already been reported earlier,[15] these data are used in **Table 2** and **3** as well as in **Figure 2, 3, 4, 5**, and **6**.

**Table 2.** Extracted optical properties as measured in 0.1 mM chloroform solution.

	Extinction			Luminescence		
	$\lambda_{a,e}$ [nm]	Opt. gap [eV]	f	Edge [nm]	Peak [nm]	Φ [%]
IP1	454	2.73	0.09	401	481	9
IP2	438	2.83	0.09	407	473	8
IP3	459	2.70	0.16	401	444	9
IP4	433	2.86	0.10	408	479	11
IP5	427	2.90	0.16	410	467	12
IQ1	424	2.92	0.17	417	473	30
IQ2	421	2.95	0.19	411	463	14
IQ3	430	2.88	0.27	412	460	28
IQ4	423	2.93	0.23	418	476	28
IQ5	432	2.87	0.23	414	467	35

Table 3. Photoluminescence properties of crystals and TFs.

	TF absorption		TF luminescence		Crystal luminescence	
	Edge [nm]	Opt. gap [eV]	Edge [nm]	Peak [nm]	Edge [nm]	Peak [nm]
IP1	–	–	–	–	417	472
IP2	443	2.80	413	489	427	489
IP5	434	2.86	419	488	420	496
IQ3	446	2.78	427	484	429	484
IQ4	436	2.84	420	498	430	512
IQ5	448	2.77	421	485	445	491

1900677 (2 of 10)
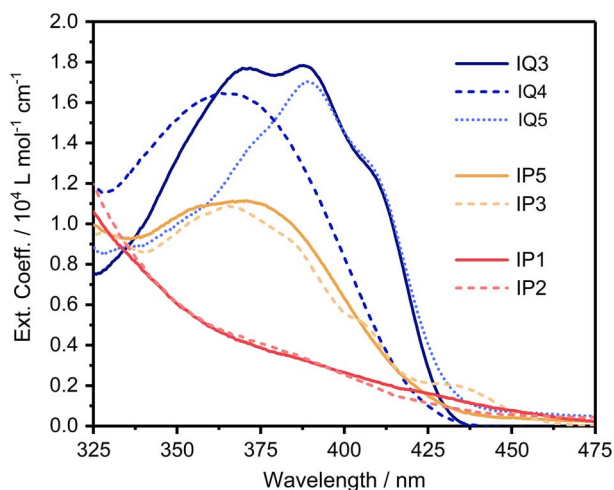
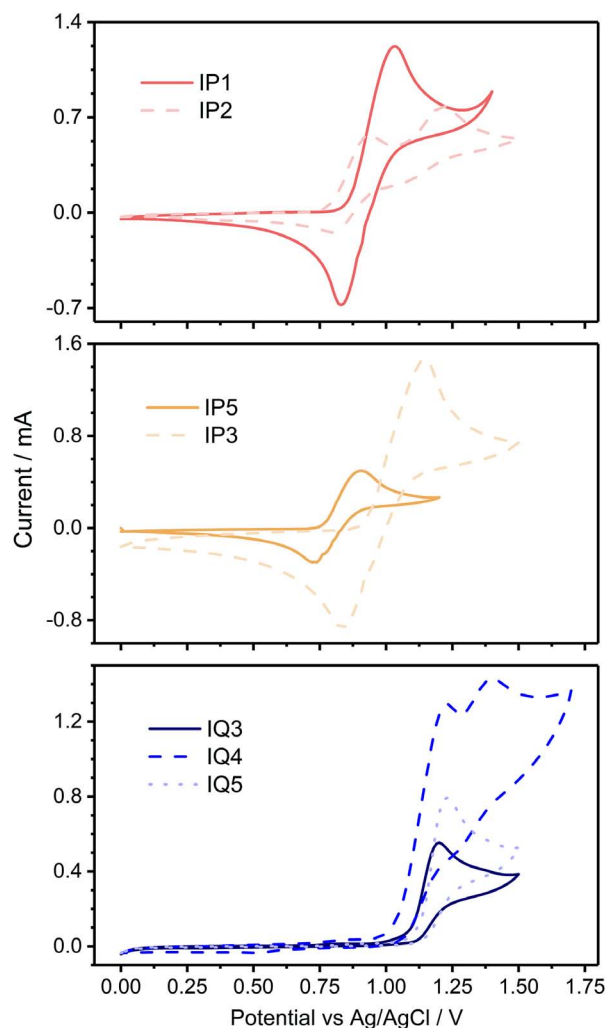**Figure 2.** Extinction spectra of exemplary molecules as measured in 0.1 mM chloroform solution.
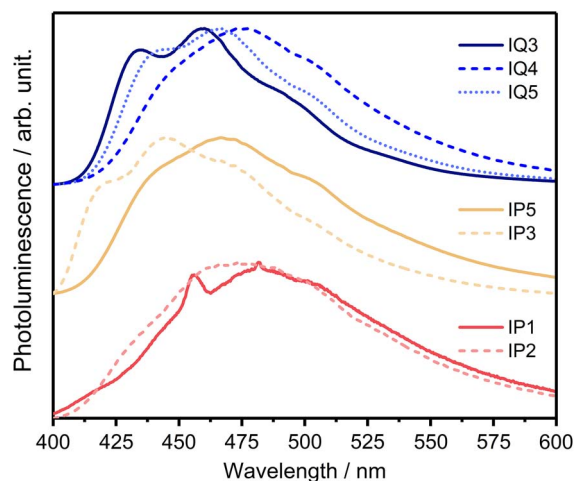
Figure 3. Normalized and offset photoluminescence spectra of exemplary molecules in 0.1 mM chloroform solution.

Figure 4. Cyclic voltammograms of exemplary molecules (5 mM) in 0.1 M TBABF$_4$/DMF solution at a scan rate of 50 mV s^{-1}.

To investigate optical properties, light extinction and photoluminescence measurements were carried out. Chloroform as a solvent has been shown to be suitable for such experiments, as it dissolves most of the target molecules, but it does not significantly influence electronic and optical properties.[36]

2.1. Structure and Energy Levels of Isolated Molecules

Figure 2 shows exemplary extinction spectra (see Figure S2, Supporting Information, for other spectra), and the extracted properties of all molecules investigated are shown in Table 2. The optical gap energy was obtained by a linear fit of the extinction edge $\lambda_{a.e}$ and converting the intersection wavelength into an energy value.[36] The oscillator strength of the absorption process, depending on the transition dipole moment and overlap of the initial- and final-state wave functions, was determined by integration of the spectra from 2 to $3 \times 10^4\,\text{cm}^{-1}$ (500–333 nm)

and calculated according to $f = 4.32 \times 10^{-9}/n \times \int \varepsilon(\nu)\text{d}\nu$.[36] As a starting point, **IP1** shows a broad, flat extinction with no clear maximum. An oscillator strength of $f = 0.09$ is derived and the transition is, thereby, assigned to a π–π^* transition.[37] The introduction of a methoxy group for **IP2** has no significant effect on absorption. Increasing the aromatic system R to a naphthalenyl moiety, e.g., for **IP4** leads to a small increase to $f = 0.10$.

Upon introduction of a pyridyl moiety, f significantly increases, as is the case when comparing **IP1** with **IP3** or **IP4** with **IP5**. The molecular conformation in the ground state calculated by DFT and the corresponding frontier orbital wave functions are shown in **Figure 7** for a representative group of molecules (see Figure S3 and S4, Supporting Information, for data of other compounds). The introduction of a nitrogen atom at position 2 into R or R′ (**IP3**, **IP5**, **IQ2**, **IQ3**, and **IQ5**) leads to a planarization of this peripheral moiety with the core of the molecule, which is presumably due to the missing repulsion of the hydrogen atom previously bound to the replaced carbon. In addition, a small interaction between the lone pair of nitrogen and the neighboring hydrogen atom at the core might support the
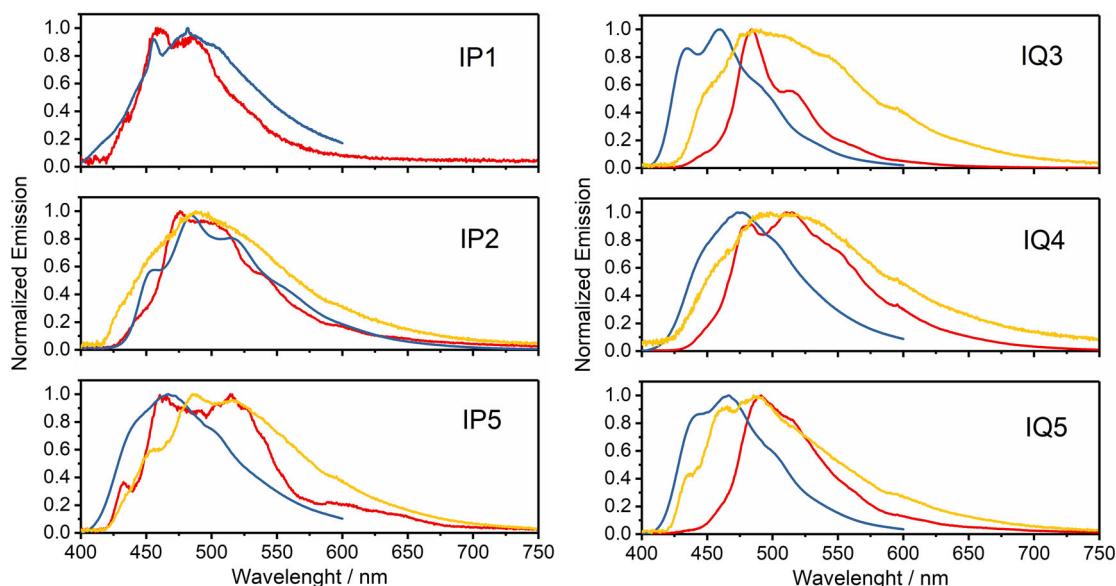
Figure 5. Photoluminescence spectra in solution (blue line), of crystals (red line), and of thin-film samples (yellow line).
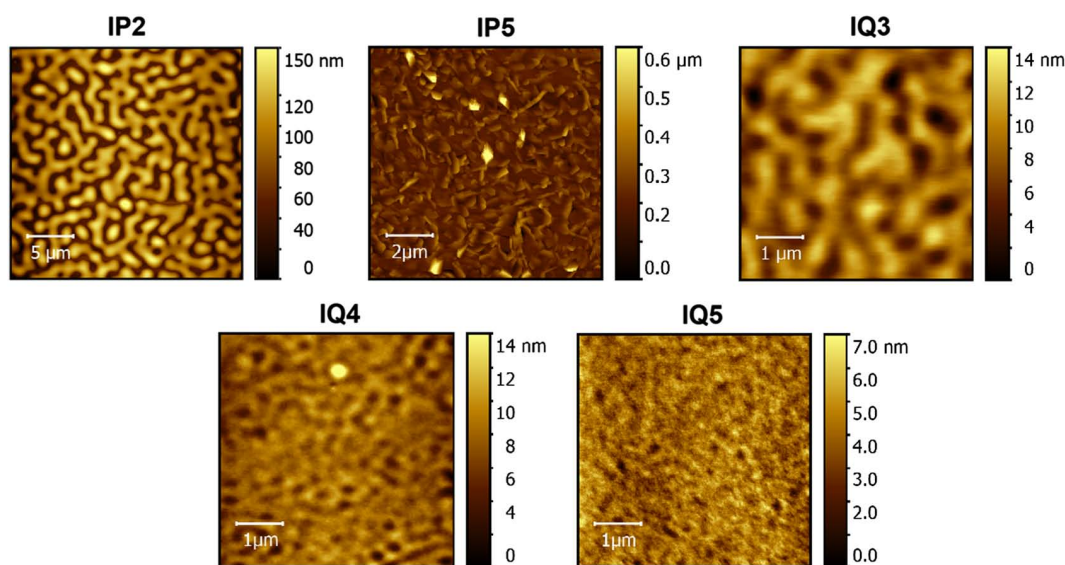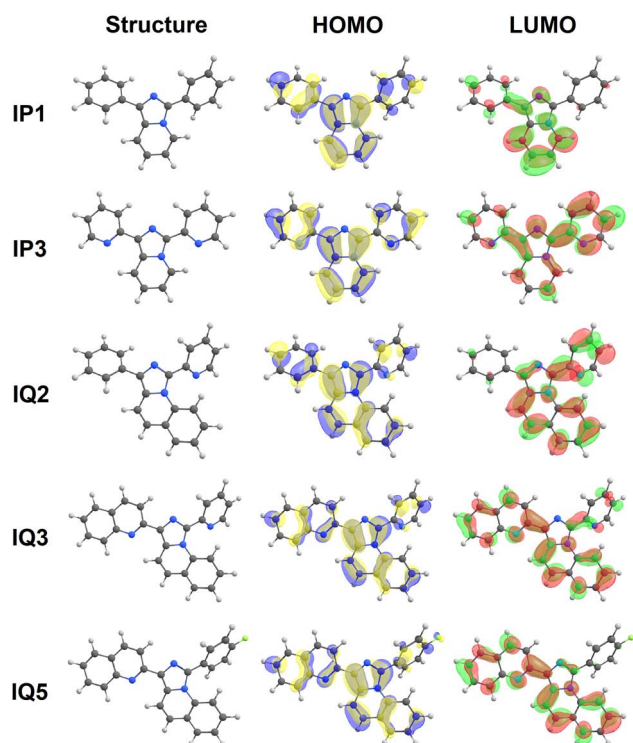

Figure 6. AFM images of surfaces for TFs of molecules **IP2**, **IP5**, **IQ3**, **IQ4**, and **IQ5**.

planarization. An example is shown for **IP1** and **IP3** in Figure 7. Planarization directly influences the magnitude of the transition dipole by increasing orbital distribution and/or overlap of the wave functions for ground and excited states. In the case of **IP1**, the HOMO is spread over the whole molecule, whereas the calculated empty lowest-unoccupied molecular orbital (LUMO) as an approximation for the excited state is located on one of the twisted side groups, R or R′ only. For **IP3**, the π-orbitals on R′ are in plane and the LUMO is extended to both peripheral pyridyl groups. The optical gaps for all IPs are roughly identical at 2.80 ± 0.08 eV.

When exchanging the IP to an IQ, as can be seen from **IP4** to **IQ1**, f increases significantly, which can be further improved by the introduction of nitrogen atoms at position 2 in R and R′ (see **IQ1–IQ3**). DFT calculations show that R′ is twisted out of the imidazo plane for all IQs studied, as there is a hindrance by the hydrogen atom at position 6 on the core (Figure 1) for the R′ side group to be planar (**IQ5** in Figure 7). Both HOMO and LUMO are mainly centered on an axis from R along the core of the molecule. The hydrogen atom at position 2 of R′ with 4-fluoro-phenyl moiety leads to a further twist of R′, whereas with a pyridyl group at R′ (**IQ3** and **IQ2**), frontier orbitals include the side group. In case of **IQ2**, the LUMO even shifts from R to R′. The optical gap at 2.91 ± 0.03 eV does not significantly change among the IQs investigated and is slightly larger than that for the smaller pyridine IP homologue.

**ADVANCED
SCIENCE NEWS**

www.advancedsciencenews.com

pssb

physica status solidi

www.pss-b.com

	Structure	HOMO	LUMO
IP1			
IP3			
IQ2			
IQ3			
IQ5			

Figure 7. Calculated molecular structure and frontier orbitals of exemplary molecules.

Exemplary photoluminescence spectra (see Figure S2, Supporting Information, for spectra of other compounds) are shown in Figure 3. The emission edges determined by a linear fit and the peak position are shown in Table 2 together with the quantum yield Φ. The emission spectra resemble each other, with their edge at 410 ± 6 nm, following the trend given by the respective absorption edge. Molecules with a nitrogen-containing moiety at R are observed to have a spectrum shifted toward higher energies. Presumably, a more rigid molecular conformation leads to such a higher energy of the excited state.

The emission quantum yield Φ closely follows the trend given by f, when comparing IPs with IQs. The intensity of emission depends on the population of the excited state, which is a direct consequence of absorption intensities at constant rates of nonradiative deactivation processes. In the absence of deactivation processes, the lifetime of an excited state can be approximated by the Strickler–Berg relationship.[38] In cases of low Φ at high f, observed for **IP3**, **IP5**, **IQ2**, and to a lesser extent **IQ3**, nonradiative excited state deactivation is present to a larger extent than in the case of **IQ1**, **IQ4**, and **IQ5**. Therefore, the introduction of a nitrogen atom at R′ is seen to increase nonradiative recombination.

In the context of an application in organic electronics, information on absolute energy-level positions is needed for an optimum choice of contact materials, if charges are to be injected into the material. To estimate the HOMO, the oxidation onset potential $E_{\text{onset}}^{\text{ox}}$ was measured in cyclic voltammetry experiments calibrated with and referred to an internal ferrocene (Fc) standard.[39] The onset potential was then converted according to its relationship to the ionization energy

E_i: $E_{\text{HOMO}} \approx E_i \approx -(4.6\,\text{eV} + 1.4 \cdot E_{\text{onset}}^{\text{ox}})$.[40] Exemplary cyclic voltammograms are shown in Figure 4 (see Figure S1, Supporting Information, for data of other compounds) and the results of $E_{\text{onset}}^{\text{ox}}$ and E_{HOMO} for the molecules investigated are shown in **Table 4**. The values for E_{HOMO}, as well as for E_{LUMO}, as a result of DFT calculations are also given. All IPs investigated show chemically reversible oxidation waves, assuming rather constant kinetic hindrance in both forward and backward waves. A good estimate of the equilibrium potential can be obtained by the average of peak potentials $E^{\text{ox}} \approx (E_p^{\text{ox}} + E_p^{\text{red}})/2$, which are also shown in Table 4. As this method, however, cannot be applied for IQs, the discussion is based on the values of $E_{\text{onset}}^{\text{ox}}$. The oxidation onset of IPs is found at 480 ± 57 mV versus Fc/Fc$^+$ (Table 4). Details of the substitution pattern do not lead to significant differences with the exception of the methoxy moiety in **IP2**, which has a significant electron-donating effect, leading to less-positive E^{ox}, $E_{\text{onset}}^{\text{ox}}$, and an increase in HOMO energy. For **IP2**, a second oxidation wave is observed, which can be assigned to a second, reversible oxidation.

In contrast, the IQs in this study do not show chemical reversibility in their oxidation waves. Previous measurements on **IQ3** with different scan rates[15] could be explained by a chemical reaction, which removed the oxidized molecules from the electrodes and thereby hindered their rereduction.[41] The oxidation onsets of IQs are found at a higher potential of 660 ± 60 mV versus Fc/Fc$^+$, and the HOMO is found at lower energies for IQs than for the IP homologues. DFT calculations yield a HOMO concentrated along the IQ core and R, showing that by twisting R′ out of the imidazo plane a different electronic system is affected by oxidation of IQ compared with IP with their larger contribution of R′. A second oxidation is found for **IQ1** and **IQ4**, indicating that the naphthalenyl moiety is the reason when comparing with **IQ2** or **IQ5**, respectively.

The trend of calculated HOMO energies fits well with the values determined by electrochemistry with a mean difference of 135 ± 80 meV between calculation and electrochemical

Table 4. Electrochemically determined HOMO energy and calculated theoretical frontier orbital energy.

	Electrochemistry			DFT		
	$E_{\text{onset}}^{\text{OX}}$ [V][a]	E_{OX} [V][a]	E_{HOMO} −[eV]	E_{HOMO} −[eV]	E_{LUMO} −[eV]	E_{GAP} [eV]
IP1	0.50	0.37	5.30	5.24	1.47	3.77
IP2	0.39	0.34	5.15	5.09	1.40	3.69
IP3	0.56	0.46	5.38	5.27	1.53	3.74
IP4	0.50	0.39	5.30	5.18	1.54	3.64
IP5	0.45	0.37	5.23	5.21	1.55	3.66
IQ1	0.60	–	5.44	5.28	1.73	3.55
IQ2	0.73	–	5.62	5.35	1.79	3.56
IQ3	0.70	–	5.58	5.39	1.92	3.47
IQ4	0.59	–	5.43	5.38	1.85	3.53
IQ5	0.69	–	5.57	5.45	1.97	3.48

[a]Versus Fc/Fc$^+$.

ADVANCED
SCIENCE NEWS
www.advancedsciencenews.com

physica
pss status solidi
www.pss-b.com

experiment. As DFT calculations were carried out for isolated molecules without any dielectric environment and electrochemistry does include the effects of solvent and intermolecular interaction, such deviation is expected. The energy difference E_{GAP} between HOMO and LUMO (Table 4) is 3.7 ± 0.05 eV for IPs and reduced to 3.5 ± 0.04 eV for IQs. Such a clear trend is remarkable in view of the variety of substituents. The decrease in E_{GAP} indicates an increased delocalization of electrons in the π-system of the studied IQs, which is expected in view of the increased ring size.

The experimental optical absorption gap of both homologues (Table 2) is found at 2.80 ± 0.08 eV for IPs and is slightly larger for IQs with 2.91 ± 0.03 eV. A comparison with the values of E_{GAP} suggests a stronger stabilization of the electronically excited state in IPs compared with IQs.

2.2. Structure and Electronic Coupling in Crystals and Thin Solid Films

For a discussion of application in organic electronics, solid-state properties are of prominent interest. Therefore, crystals were grown to study such highly ordered assemblies of molecules. Entrainer sublimation produced crystals of **IP5**, **IQ3**, **IQ4**, and **IQ5**. The crystals of **IP1** and **IP2** were obtained by solvent diffusion. Crystal structures could be determined by X-ray diffraction (XRD) for **IP1**,[42] **IP2**,[43] **IQ3**,[15] **IQ4**,[16] and **IQ5**,[16] and unit cells are shown in **Figure 8**. The density of molecules in the crystal lattice is 1.332 g cm^{-3} for **IP1**, 1.333 g cm^{-3} for **IP2**, whereas **IQ3**, **IQ4**, and **IQ5** exhibit a density of 1.390, 1.412, and 1.421 g cm^{-3}, respectively. The molecular conformation found in unit cells shows that the structure optimized for isolated molecules (Figure 7) is widely preserved in the solid state (Figure 8), speaking in favor of rather small intermolecular lattice energies compared with intramolecular binding energies. The twisting of R′ in case of the IQs as well as planarization of R or R′ for pyridyl and quinolinyl moieties is observed, demonstrating the stability of individual molecular conformation in the presence of intermolecular interactions. For **IP1** and **IP2**, both R and R′ are twisted out of plane, whereas, for example, R on **IQ5** is almost in plane with the quinoline core. A similar behavior is seen for R and R′ on **IQ3**[15] in comparison with **IQ4**.

In the crystal lattice of **IP1**, the molecules are all facing in the same direction, so IP cores are aligned in a row. In the orthogonal direction of the cores, e.g., in the direction of π-orbitals, **IP1** molecules are not stacking cofacial, as one molecule is shifted by half a core length from direct overlap, leading to parallel displacement. For **IP2**, IP cores of adjacent molecules are roughly oriented toward each other but are not parallel regarding their π-systems. These planes are separated by R′, whose phenyl moieties are also not parallel to each other. A parallel displaced structure is observed. The crystal structure of **IQ3** was previously found to have IQ cores and R of adjacent molecules stacked cofacial but in two planes almost orthogonal to each other.[15] An almost parallel, cofacial arrangement of IQ cores and R is also observed for all molecules in the **IQ4** and **IQ5** structure, however, with a rotated R′ in between. Separation of the two molecules in the unit cell is dependent on the degree of twist for R; they are closer for **IQ5** than for **IQ4**. Planarization in the imidazo plane, therefore, has a significant influence on crystal structure. As the imidazo plane represents the plane of the frontier orbitals (Figure 7), such a molecular arrangement in the unit cells of IQs leads to a preferentially parallel arrangement of HOMO and LUMO. Such an interaction of π-orbitals can serve to stabilize the structure.

The photoluminescence of crystals was investigated by fluorescence microscopy. Figure 5 shows the results in comparison with emission in chloroform solution and thin-film samples on quartz, whereas Table 3 shows the results. Earlier work has shown a strong red-shift of photoluminescence for crystals of **IQ3** from spectra measured in solution, indicating a clear influence of molecular coupling in the crystal. A similar behavior is found for **IQ4** and **IQ5**, which is plausible in view of the similar, intermolecular arrangement, in particular, of the π-orbitals, which determines the strength of coupling. In consequence, **IQ5** displays a stronger red-shift than **IQ4**, corresponding well to the smaller distance between molecules of **IQ5** in the unit cell.

IP1, **IP2**, and **IP5** do not display red-shifted emission. In case of **IP1** and **IP2**, this can be explained by a nonparallel molecular arrangement, which might also be the case for **IP5** (no structure obtained). It is seen that a comparison of crystal photoluminescence compared with that in solution can be utilized to show the degree of intermolecular coupling in the crystal structure. Such coupling is important for organic electronics to discuss charge transport. TFs of molecules **IP2**, **IP5**, **IQ3**, **IQ4**, and **IQ5**, as typical for application in organic electronics, were prepared under identical experimental parameters by PVD. The photoluminescence of these TFs is shown in Figure 5.

For **IP2** and **IP5** TFs, the spectral shape of the photoluminescence is similar to that of crystals (and solution); missing, however, are the pronounced features of vibrational modes or optical interference in the crystals. In case of **IQ3**, the thin-film emission spectrum is also red-shifted, compared with that in solution, as seen in a previous work.[15] For **IQ4** and **IQ5**, the spectrum of the TF is centered at a comparable wavelength to that found for the crystal, with its edge close to the spectrum of the solution, indicating weaker coupling in the TF. In all cases, the emission of TFs is broader and does present less-distinct
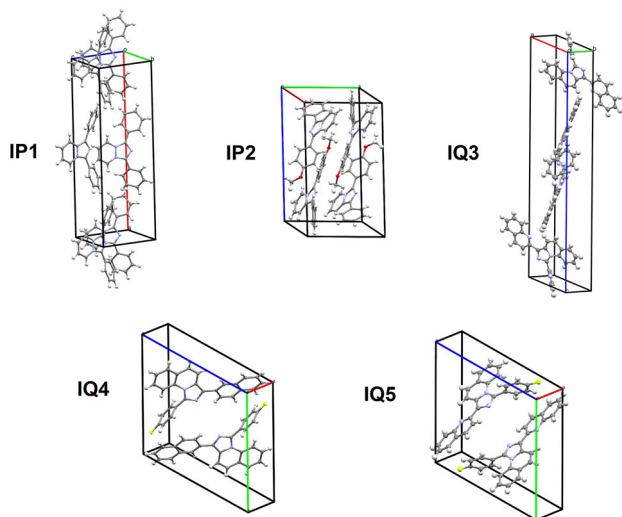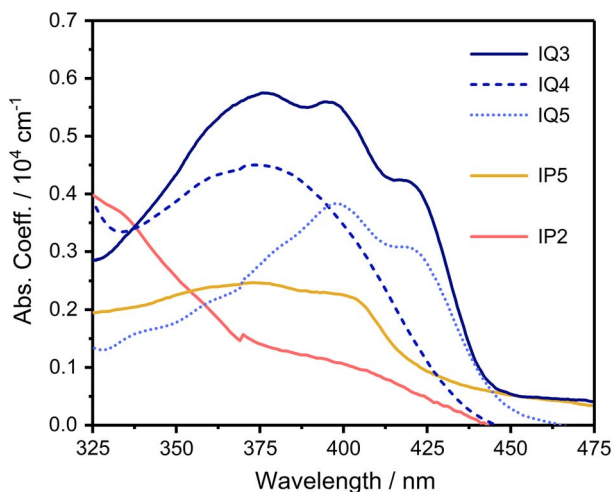

Figure 8. Arrangement of molecules in the unit cells as determined by XRD.

vibrational features, which is either caused by amorphous or polycrystalline film structures.

AFM (Figure 6) was used to obtain further information on thin-film morphology for **IP2**, **IP5**, **IQ3**, **IQ4**, and **IQ5**. **IP5**, at 214 nm film thickness, exhibits plate-like domains with well-defined straight borders reminiscent of crystalline growth. The other TFs show a smoother, more amorphous surface morphology. **IP2** at 63 nm film thickness forms a net structure found before for **IQ3** at a similar thickness, which then grew to show a smooth, closed film, as shown again in Figure 6 at 153 nm.[15] **IQ4** and **IQ5** exhibit a similar surface at 160 and 82 nm, respectively. An amorphous film structure is, therefore, proposed for **IP2**, **IQ4**, and **IQ5**, as well as **IQ3**, fitting to the spectral broadening seen in a comparison of crystal and thin-film photoluminescence.

Thin-film absorption (**Figure 9**) was measured and normalized to film thickness. The optical gap of TFs gets smaller by about 10 meV for **IQ3**, **IQ4**, and **IQ5**, compared with the values determined from the dissolved molecules in good correspondence to the shifts observed in the photoluminescence of TFs and also of crystals, all caused by specific intermolecular coupling in solid IQs. For **IP2** and **IP5**, no such reduction in the optical gap is found. The absorption coefficients of TFs follow the same general trend as the molar extinction coefficients in solution (Figure 2), IQs > **IP5** > **IP2**. However, when looking in detail, some consequences of intermolecular coupling in TFs become apparent. Comparing **IQ3**, **IQ4**, and **IQ5**, which in solution do show similar extinction, the TF of **IQ3** has a much higher absorption coefficient. A comparison of the molar volume of IQs in the crystal lattices does not display significantly closer packing for **IQ3** (267.9 $cm^3 mol^{-1}$ for **IQ3**, 275.1 $cm^3 mol^{-1}$ for **IQ4**, and 274.1 $cm^3 mol^{-1}$ for **IQ5**). Assuming, therefore, a similar trend of density in the amorphous TFs, and a similar influence of the dielectric environment, the increased absorption of **IQ3** is presumably caused by a specific coupling of chromophores in the solid.

The determination of the excited state lifetime in solid samples gives direct access to the influence of solid-state effects on photoluminescence when compared with that of dissolved molecules. Fluorescence decay in solution was fitted with a monoexponential decay function, whereas TFs had to be fitted by a biexponential decay to obtain satisfactory precision. Results are shown in Figure S5, Supporting Information, and in **Table 5**. The average lifetime in the TFs of **IP2**, **IP5**, **IQ4**, and **IQ5** is slightly decreased when compared with measurements in solution. Presumably, this is due to an increase in nonradiative decay caused by intermolecular interaction. For **IQ3**, the excited state lifetime is significantly lower in the solid. This might be caused by an even higher nonradiative decay rate than for other IQs. Alternatively, the short lifetime of the excited state of **IQ3** could stem from a higher radiative rate. In solution, **IQ3** has the highest f among IQs and absorption of **IQ3** TFs was even found to be increased in relation to the other IQs studied (Figure 9), suggesting a positive influence of solid-state interaction on the radiative rate.

As a first step to show the applicability of the studied class of molecules in electro-optical devices, a prototype OLED structure was prepared with **IQ5**, which shows the highest molecular photoluminescence quantum yield (Table 2). Suitable contact materials, able to inject charge carriers, fitting to the frontier orbital energies and a layer architecture already developed for **IQ3**[18] have been used, and a model device ITO/PEDOT:PSS/**IQ5**/BCP/Al has been prepared by spin coating (PEDOT:PSS) and PVD (all other layers) on a commercial indium tin oxide (ITO) substrate. The results of this test OLED with **IQ5** as an active emitting layer are shown in **Figure 10**. The spectrum obtained does fit well to the photoluminescence signal found for the corresponding TF regarding peak position and shape, no signals specific for crystalline domains or isolated molecules are seen beyond this. It is thereby shown that the amorphous arrangement of molecules, which is dominant in TFs, can also be electrically addressed and work as an emitter layer. This was also seen before for **IQ3** in the same contacting scheme.[18] The diode produces blue/greenish-white electroluminescence at stable electrical performance and reasonable current density (the inset in Figure 10). Its emission color according to the CIE 1931 XYZ color space with a 2° observer is found at $x = 0.27$, $y = 0.36$, and $z = 0.37$. The visual impression looks similar to the observed photoemission (see photographs in Table of Contents figure). The rather high value of the threshold voltage, as also previously seen for **IQ3**, indicates high barriers for charge carrier injection in the present test structure. Therefore, optimization of the device architecture is clearly needed and may further improve such OLEDs with IQ emitters. Nevertheless, at driving voltages

Figure 9. Absorption coefficients of TFs deposited by PVD.

Table 5. Measured excited-state lifetime of molecules at 20 µM in chloroform and of TFs.

	Solution		TF				
	τ [ns]	X^2	τ_1 [ns]	τ_2 [ns]	a	X^2	τ_{avg} [ns]
IP1	3.9	35.5	–	–	–	–	–
IP2	2.3	18.5	2.2	5.3	0.70	1.4	2.3
IP5	2.1	9.4	1.7	6.3	0.84	3.6	1.9
IQ3	1.9	6.5	0.5	5.3	0.98	3.7	0.5
IQ4	2.3	8.8	1.8	6.4	0.91	3.4	1.9
IQ5	2.3	14.5	1.3	6.3	0.72	10.6	1.8
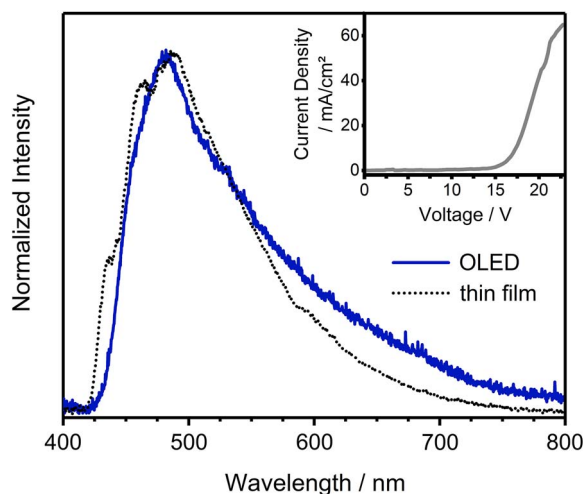
Figure 10. Electroluminescence (blue) for an OLED with **IQ5** as the emitting layer obtained at 22.5 V driving voltage. Thin-film photoluminescence (black dots, compare Figure 5) is shown for comparison. The current density/voltage characteristic of the OLED is given as an inset.

above the threshold voltage of about 16.5 V, it can be assumed that all contacts become conducting and that the emissive layer limits the current. A lower limit of the electrical conductivity of $1.2 \times 10^{-7}\,\text{S cm}^{-1}$ for **IQ5** was, therefore, determined from a fit to the linear part, which is quite common for organic semiconductors.[34]

3. Conclusion

Starting at 1,3-diphenyl imidazo[1,5-*a*]pyridine as the most simple molecule of this study, the influence of the enlarging ring size at substitutional groups R and R′, as well as when using larger IQs, was examined. Oscillator strength and quantum yield are increased and are significantly higher on IQs investigated. Quantum yields, therefore, can be improved using such a higher homologue core. In addition, pyridyl and quinolinyl moieties were introduced at R and R′, rotating side groups in plane to the fluorophore core and thereby extending frontier orbitals, as seen by DFT. This also leads to increased absorption. IQs have, thereby, been identified as a promising motif in luminescent molecules, building on the established IPs.

Cyclic voltammetry was used to investigate oxidation properties, reporting oxidation onsets and HOMO energies. IQs are more stable against oxidation yet prone to irreversible consecutive chemical reaction once oxidized. In contrast, IPs are stable in the oxidized state. Functional moieties on R and R′ were concluded to have minor effects when compared against an increase in electron binding from $-5.27 \pm 0.08\,\text{eV}$ for IPs to $-5.53 \pm 0.08\,\text{eV}$ for IQs. The quantum chemical calculations reproduce the trend, showing a change in HOMO and LUMO locations from being spread over most of the IP molecule to an axis of core to R on the larger IQ homologues. Furthermore, frontier orbitals of the investigated IQs are located mainly on an axis of the fluorophore core and R due to a rotation of R′.

Such conformation is supported by single-crystal XRD. In the crystals, the molecules are stacked with this axis in parallel.

In consequence, the crystals of IQs exhibit a large red-shift of photoluminescence compared with isolated molecules in solution. This can be assigned to intermolecular coupling and is not observed for the investigated IPs. TFs also exhibit intermolecular coupling, but to a lesser extent, which is reaffirmed by a shift of absorption spectra relative to those in solution. The decrease is attributed to an amorphous film structure in most cases, deduced from a broadening of photoluminescence spectra. In confirmation, AFM reveals smooth, amorphous TFs of **IP2**, **IP4**, and **IQ5**, similar in film morphology to **IQ3**. **IQ3** is found to be the strongest absorber for thin-film samples because of the specific intermolecular coupling of chromophores. **IQ5**, however, does possess a higher molecular fluorescence quantum yield. An OLED test structure containing **IQ5** as the emitter layer was built, demonstrating its feasibility in such device architectures. In conclusion, IQs have been proven as attractive structural motifs, allowing further molecular optimization and advanced device engineering.

4. Experimental Section

The molecules **IP1** (1,3-diphenylimidazo[1,5-*a*]pyridine), **IP2** (3-(4-methoxyphenyl)-1-(phenyl)imidazo[1,5-*a*]pyridine), **IP3** (1,3-di(pyridin-2-yl)imidazo[1,5-*a*]pyridine), **IP4** (1-(naphthalenyl)-3-(phenyl)imidazo[1,5-*a*]pyridine), **IP5** (1-(naphthalenyl)-3-(pyridin-2-yl)imidazo[1,5-*a*]pyridine), **IQ1** (1-(naphthalenyl)-3-(phenyl)imidazo[1,5-*a*]quinoline), **IQ2** (3-(pyridin-2-yl)-1-(phenyl)imidazo[1,5-*a*]quinoline), **IQ3** (1-(pyridin-2-yl)-3-(quinolin-2-yl)imidazo[1,5-*a*]quinoline), **IQ4** (3-(4-fluorophenyl)-1-(2-naphthalenyl)imidazo[1,5-*a*]quinoline), and **IQ5** (3-(4-fluorophenyl)-1-(2-quinolinyl)imidazo[1,5-*a*]quinoline) were synthesized as described by Albrecht et al.[15] and purified by sublimation in high vacuum. Extinction measurements in the ultraviolet and visible spectral region (UV–vis) of solutions were carried out with a JASCO V-760 spectrometer at 10 µM concentration in chloroform. The corresponding emission properties were investigated with a Jasco Germany FP-8300 spectrometer. The fluorescence quantum yield (Φ) of the materials was measured in chloroform ($n = 1.445$)[44] calibrated against an equally concentrated quinine sulfate solution ($\Phi = 0.546$ and refractive index $n = 1.339$).[45] Fluorescence lifetime measurements were carried out on 20 µM solutions of the molecules in chloroform. A scattering solution of ZnO nanoparticles (40 nm diameter) was used to obtain the instrument response function (IRF). In case of thin-film measurements, a roughened Ted Pella Inc. GE124 quartz glass slide served as the scattering probe instead. An IBH FluoroCube was used with a 370 nm IBH LED as the excitation source and a 380 nm bandpass filter. DecayFit 1.3 was used for data analysis and fitting.[46] Solution data were fitted with a single-exponent decay function $y = \exp(-t/\tau)$ and thin-film data were fitted with a second term according to $y = a \cdot \exp(-t/\tau_1) + (1 - a) \cdot \exp(-t/\tau_2)$. For cyclic voltammetry, a 5 mM dimethylformamide (DMF) solution (Carl Roth GmbH) of the analyte using 0.1 M tetrabutylammonium tetrafluoroborate (TBABF$_4$, Sigma Aldrich) as a supporting electrolyte was prepared. Platinum wires were used as the working and counter electrodes and a leak-free Ag/AgCl electrode (LF-2, Warner Instruments) as the reference electrode. Ferrocene (Fc) (Sigma Aldrich >98%) was used as internal reference. All electrochemical measurements were carried out in a water and oxygen-free environment (<0.5 ppm) with an Ivium Technologies IviumStat potentiostat at 50 mV s^{-1} scan rate. The molecular full-geometry optimizations by DFT, without symmetry restrictions, were conducted using the Gaussian 16 Revision B.01 software package with the hybrid exchange correlation functional *B3LYP*[47–49] and a *def2-TZVP*[50,51] basis set. Crystals were prepared either by solvent evaporation or by entrainer sublimation in a KOYO Thermo Systems Co. Ltd. KTF030N oven. TFs were prepared in a Jeol JEE-400 vacuum evaporator by PVD or in a self-made evaporation chamber under high vacuum. The material was evaporated

from a resistively heated crucible at evaporation rates of about 1 nm min^{-1}, measured in situ by a quartz crystal microbalance (QCM). TFs of **IP1** could not be deposited by this method. AIST-NT SmartSPM with Seiko Instruments SEIHR tips was used for all AFM measurements, analyzed by GWYDDION 2.47. The average film thickness was determined mainly by AFM. In case of **IP2**, the grains of materials, seen in the scan shown in Figure 6, were marked and their volume converted to that of a uniform film, with a rectangular cross-section of the same volume. Film thickness of **IQ3** was determined by QCM using a film density of 1.5 g cm^{-3}.[15] As an approximation for the crystalline film of **IP5**, the minimum of all available data points was set to zero, assuming to be the quartz glass surface. The maximum of height distribution was then interpreted as average film thickness. In case of **IQ4** and **IQ5**, the films were scratched by a plastic spatula, exposing the quartz surface. The film thickness was then measured by averaging the height obtained from line scans of the edge. Thin-film absorbance was investigated with an Analytics Jena Specord 40 UV/vis spectrometer. The emission of TFs and crystals was measured in a fluorescence microscope with a Hamamatsu Photonics PMA-12 CCD spectrometer at 365 nm excitation from a mercury lamp through an optical filter. OLED preparation was adopted from a previous work[17]. Bathocuproine (BCP, (>99.99%) and poly(3,4-ethylenedioxythiophene) polystyrene sulfonate (PEDOT:PSS) were obtained from Ossila, ITO-coated glass from Zhuhai Kaivo Optoelectronic Technology Co., Ltd. Devices were structured with a layer order of ITO/PEDOT:PSS/**IQ5**/BCP/Al (180 nm/~50 nm/100 nm/20 nm/60 nm) and driven by a Keithley 2400 sourcemeter. Electroluminescence was studied with a Hamamatsu C10082CA detector through an Ocean Optics UV–vis glass fiber cord and an 8 mm-diameter lens. During measurements, the samples were cooled by a N$_2$ stream onto the Al cathode.

Supporting Information

Supporting Information is available from the Wiley Online Library or from the author.

Conflict of Interest

The authors declare no conflict of interest.

[1] G. M. van Dam, G. Themelis, L. M. A. Crane, N. J. Harlaar, R. G. Pleijhuis, W. Kelder, A. Sarantopoulos, J. S. de Jong, H. J. Arts, A. G. van der Zee, J. Bart, P. S. Low, V. Ntziachristos, *Nat. Med.* **2011**, *17*, 1315.

[2] J. Rao, A. Dragulescu-Andrasi, H. Yao, *Curr. Opin. Biotechnol.* **2007**, *18*, 17.

[3] J. Clark, G. Lanzani, *Nat. Photonics* **2010**, *4*, 438.

[4] P. Heimel, A. Mondal, F. May, W. Kowalsky, C. Lennartz, D. Andrienko, R. Lovrincic, *Nat. Commun.* **2018**, *9*, 4990.

[5] C. W. Tang, S. A. VanSlyke, *Appl. Phys. Lett.* **1987**, *51*, 913.

[6] C. Bizzarri, F. Hundemer, J. Busch, S. Bräse, *Polyhedron* **2018**, *140*, 51.

[7] N. Thejo Kalyani, S. J. Dhoble, *Renewable Sustainable Energy Rev.* **2012**, *16*, 2696.

[8] Z. Yang, Z. Mao, Z. Xie, Y. Zhang, S. Liu, J. Zhao, J. Xu, Z. Chi, M. P. Aldred, *Chem. Soc. Rev.* **2017**, *46*, 915.

[9] M. Mohan, S. Pangannaya, M. N. Satyanarayan, D. R. Trivedi, *Opt. Mater.* **2018**, *77*, 211.

[10] H.-W. Chen, J.-H. Lee, B.-Y. Lin, S. Chen, S. Wu, *Light Sci. Appl.* **2017**, *7*, 17168.

[11] D. Luo, Q. Chen, Y. Gao, M. Zhang, B. Liu, *ACS Energy Lett.* **2018**, *3*, 1531.

[12] G. Volpi, C. Garino, E. Priola, E. Diana, R. Gobetto, R. Buscaino, G. Viscardi, C. Barolo, *Dyes Pigm.* **2017**, *143*, 284.

[13] G. Volpi, G. Magnano, I. Benesperi, D. Saccone, E. Priola, V. Gianotti, M. Milanesio, E. Conterosito, C. Barolo, G. Viscardi, *Dyes Pigm.* **2017**, *137*, 152.

[14] G. Volpi, B. Lace, C. Garino, E. Priola, E. Artuso, P. C. Vioglio, C. Barolo, A. Fin, A. Genre, C. Prandi, *Dyes Pigm.* **2018**, *157*, 298.

[15] G. Albrecht, J. M. Herr, M. Steinbach, H. Yanagi, R. Göttlich, D. Schlettwein, *Dyes Pigm.* **2018**, *158*, 334.

[16] J. M. Herr, C. Rössiger, G. Albrecht, H. Yanagi, R. Göttlich, *Synthesis* **2019**, unpublished.

[17] G. Volpi, C. Garino, E. Conterosito, C. Barolo, R. Gobetto, G. Viscardi, *Dyes Pigm.* **2016**, *128*, 96.

[18] G. Albrecht, C. Geis, J. M. Herr, J. Ruhl, R. Göttlich, D. Schlettwein, *Org. Electron.* **2019**, *65*, 321.

[19] A. Marchesi, S. Brenna, G. A. Ardizzoia, *Dyes Pigm.* **2019**, *161*, 457.

[20] D. R. Mohbiya, N. Sekar, *ChemistrySelect* **2018**, *3*, 1635.

[21] F. Shibahara, E. Yamaguchi, A. Kitagawa, A. Imai, T. Murai, *Tetrahedron* **2009**, *65*, 5062.

[22] F. Shibahara, R. Sugiura, E. Yamaguchi, A. Kitagawa, T. Murai, *J. Org. Chem.* **2009**, *74*, 3566.

[23] Y. Yamaguchi, Y. Matsubara, T. Ochi, T. Wakamiya, Z.-I. Yoshida, *J. Am. Chem. Soc.* **2008**, *130*, 13867.

[24] Y. Y. Pan, J. Huang, Z. M. Wang, D. W. Yu, B. Yang, Y. G. Ma, *RSC Adv.* **2017**, *7*, 26697.

[25] H. Meier, U. Stalmach, H. Kolshorn, *Acta Polym.* **1997**, *48*, 379.

[26] J. E. Norton, K. N. Houk, *J. Am. Chem. Soc.* **2005**, *127*, 4162.

[27] Z.-F. Yao, J.-Y. Wang, J. Pei, *Cryst. Growth Des.* **2017**, *18*, 7.

[28] X. Yang, L. Wang, C. Wang, W. Long, Z. Shuai, *Chem. Mater.* **2008**, *20*, 3205.

[29] J. Clark, C. Silva, R. H. Friend, F. C. Spano, *Phys. Rev. Lett.* **2007**, *98*, 206406.

[30] S.-J. Yoon, S. Varghese, S. K. Park, R. Wannemacher, J. Gierschner, S. Y. Park, *Adv. Opt. Mater.* **2013**, *1*, 232.

[31] Z. Yang, Z. Mao, X. Zhang, D. Ou, Y. Mu, Y. Zhang, C. Zhao, S. Liu, Z. Chi, J. Xu, Y.-C. Wu, P.-Y. Lu, A. Lien, M. R. Bryce, *Angew. Chem. Int. Ed.* **2016**, *55*, 2181.

[32] H. Uratani, S. Kubo, K. Shizu, F. Suzuki, T. Fukushima, H. Kaji, *Sci. Rep.* **2016**, *6*, 39128.

[33] C. D. Dimitrakopoulos, P. R. L. Malenfant, *Adv. Mater.* **2002**, *14*, 99.

[34] S. R. Forrest, *Nature* **2004**, *428*, 911.

[35] D. Chen, S.-J. Su, Y. Cao, *J. Mater. Chem. C* **2014**, *2*, 9565.

[36] J. C. S. Costa, R. J. S. Taveira, C. F. R. A. C. Lima, A. Mendes, L. M. N. B. F. Santos, *Opt. Mater.* **2016**, *58*, 51.

[37] A. Köhler, H. Bässler, *Electronic Processes in Organic Semiconductors*, Wiley-VCH, Weinheim, Germany **2015**.

[38] S. J. Strickler, R. A. Berg, *J. Chem. Phys.* **1962**, *37*, 814.

[39] J. Pommerehne, H. Vestweber, W. Guss, R. F. Mahrt, H. Bässler, M. Porsch, J. Daub, *Adv. Mater.* **1995**, *7*, 551.

[40] B. Dandrade, S. Datta, S. Forrest, P. Djurovich, E. Polikarpov, M. Thompson, *Org. Electron.* **2005**, *6*, 11.

[41] N. Elgrishi, K. J. Rountree, B. D. McCarthy, E. S. Rountree, T. T. Eisenhart, J. L. Dempsey, *J. Chem. Educ.* **2017**, *95*, 197.

[42] CCDC: 1895170 contains the supplementary crystallographic data.

[43] CCDC: 1895166 contains the supplementary crystallographic data.

[44] S. Kedenburg, M. Vieweg, T. Gissibl, H. Giessen, *Opt. Mater. Express* **2012**, *2*, 1588.

[45] A. M. Brouwer, *Pure Appl. Chem.* **2011**, *83*, 2213.

[46] DecayFit - Fluorescence Decay Analysis Software 1.3, FluorTools, www.fluortools.com (accessed: May 2018).

[47] A. D. Becke, *J. Chem. Phys.* **1993**, *98*, 5648.

[48] B. Miehlich, A. Savin, H. Stoll, H. Preuss, *Chem. Phys. Lett.* **1989**, *157*, 200.

[49] C. Lee, W. Yang, R. G. Parr, *Phys. Rev. B* **1988**, *37*, 785.

[50] F. Weigend, R. Ahlrichs, *Phys. Chem. Chem. Phys.* **2005**, *7*, 3297.

[51] F. Weigend, *Phys. Chem. Chem. Phys.* **2006**, *8*, 1057.

1900677 (10 of 10)